

On the stabilizing effect of Solar Radiation Pressure in the Earth-Moon system

Marc Jorba-Cuscó^a, Ariadna Farrés^b, Àngel Jorba^a

^a*Departament de Matemàtiques i Informàtica, Universitat de Barcelona, Barcelona, Spain*

^b*Goddard Planetary Heliophysics Institute, University of Maryland Baltimore County, Baltimore, United States*

Abstract

Solar sails change the natural dynamics of systems: The typical trajectories are displaced and changed because of the effect of Solar Radiation Pressure (SRP). Moreover, if the effectivity of the sail is large enough, the instability of certain orbits can be diminished and even removed. In this paper we modify two models for the motion of a probe in the Earth-Moon system that include the effect of Sun's gravity to take also into account the effect of SRP. These models, the Bicircular Problem (BCP) and the Quasi-Bicircular Problem (QBCP), are periodic perturbations of the Earth-Moon Restricted Three Body Problem (RTBP). The models are modified to consider the effect of the SRP upon a Solar Sail. We provide examples of periodic orbits that are stabilized (or made less unstable) due to the effect of SRP.

Keywords: Stability, Solar Radiation Pressure, Halo orbit, continuation, dynamical equivalents

Nomenclature

μ	Moon's mass
m_S	Sun's mass
a_S	Sun's semi-major axis
ω_S	Sun's frequency
T_S	Sun's period
α_i	periodic functions defining QBCP
β	effectivity of the sail
δ	vertical pitch of the sail
α	horizontal pitch of the sail

1. Introduction

The motion of a test particle in the proximity of Earth and Moon is a hot topic in astrodynamics. The list of potential applications (see, for instance, [1, 2, 3]) that could be benefited from a deep understanding of the natural dynamics near Earth and Moon is long and it is increasing day by day. Let us mention, for instance, the possibility of setting of an extraterrestrial hub, the exploration in-situ of natural resources, deep space exploration by means of telescopes, new solutions for the del-

icate issue of space debris, end-of-life strategies adapted to the natural dynamics and, probably the most recent examples, the study of mini-moons, small objects captured (temporarily) which orbit around Earth.

A correct understanding of the natural dynamics of the Earth-Moon system is a key ingredient for preliminary steps of any kind of mission. If a certain spacecraft is endowed with a Solar Sail, the effect of SRP can change the natural dynamics substantially.

The simplest model that describes the motion of a small particle in the Earth-Moon system is the Restricted Three Body Problem (RTBP). The very specific properties of the Earth-Moon system, such as the eccentricity of the motion of the primaries or the uniformly large effect of Sun's gravity, are certainly not well captured by the Earth-Moon RTBP. It is natural, therefore, to look for a more sophisticated model. Sun's gravitational acceleration upon the test particle is the most relevant force ignored by the RTBP in a large vicinity of Earth and Moon. In this situation, the gravity of Sun acts as a periodic perturbation of the RTBP.

As a result of this perturbation, the Lagrangian points are no longer equilibria but they are replaced by periodic orbits with the same period as Sun. In general, those periodic orbit, as invariant structures, are much more unstable than their counterparts in the RTBP. Moreover, the effect of Sun is uniformly large near the triangular

points and suffices to produce bifurcations the invariant structures. In particular, the periodic orbit that replaces L_4 (and L_5) is unstable. With all these considerations, one can say that Sun acts as an unstabilizing agent in the Earth-Moon system.

As Sun is considered to be a punctual mass, the SRP effect is an inverse squared law that acts in the opposite direction of Sun's gravity. Therefore, when a sail is perpendicular to Sun, the effect of SRP diminishes the direct effect of Sun's gravity of the Sail. Of course, the indirect effects (such as the Coriolis effect or the non-constant distance between Earth and Moon) persist. Anyhow, SRP is able to stabilize (or made less unstable) some orbits.

In this work, we consider two models that introduce Sun's gravity in different ways. The first model, the so-called Bicircular Problem (BCP) [4, 5, 6], considers only the direct effect of Sun's gravity on the test particle and not on Earth and Moon. For that reason, the three primaries, Earth, Moon and Sun, move following trajectories that do not verify Newton's laws. In particular, Earth and Moon move along a circular orbit around their centre of masses while the Earth-Moon barycentre, together with Sun, move along another (coplanar) circular orbit around the centre of masses of the whole system. The second model, the Quasi-Bicircular Problem (QBCP), is a coherent version of the BCP. Indeed, in this model, the motion prescribed to the primaries is a numerical solution of the Earth-Moon-Sun Three Body Problem which is close to bicircular, see [7, 8, 9, 10].

The acceleration of SRP upon the sail depends on three parameters, the effectivity of the sail (which captures, essentially, its area-to-mass ratio) and the horizontal and vertical pitch angles. Because the period of SRP term is the same as Sun's gravitational potential, the augmented models are, as in the case of BCP and QBCP, periodic perturbations of the RTBP. Therefore, the libration points are replaced by periodic orbits, what we call **dynamical equivalents**.

Mathematically, to put a sail in a spacecraft means to modify a classical restricted model by including the effect of SRP, see [11, 12, 13, 14, 15, 16, 17] for works concerning the Earth-Moon system and [18, 19] for the Sun-Earth. SRP modifies the natural dynamics of the model, the invariant structures change their shape, their linear normal behaviour and move around the phase space. Playing with the parameters of the sail, its effectivity and orientation, one can find out different invariant objects with different linear behaviour that can be used for, otherwise inconceivable, mission concepts.

In this paper we focus on some examples of periodic orbits that are stabilized (or made less unstable)

due to the effect of SRP. In Section 2 we explain how the augmented versions of the BCP and the QBCP are derived. Section 3 contains a review of some mathematical contents that will be used widely during the rest of the paper. Those are very well known results and definitions for the mathematical community, the section is just added for selfcontainness of the paper. Section 4 is devoted to the study of some resonant Halo orbits near L_1 and L_2 . The orbits appearing in this section have been selected in order to illustrate the phenomenon of stabilization. A deeper analysis on resonant orbits near the Lagrangian points L_1 and L_2 can be found in [20]. In Section 5 we study how the triangular points evolve with respect to the parameters of the sail and we focus on the stabilization of L_3 , leading to a stability region which is very close to Earth. Finally Section 6 is devoted to conclusions and Section 7 describes some technical details to facilitate the reproducibility of the study.

2. Dynamical models

In the present section, we discuss the models used to describe the motion of a solar sail in the Earth-Moon System. The recipe to construct such a model is, first, to select a convenient motion for the primaries: Earth, Moon and Sun and then consider the dynamics of a small particle under the gravitational effect of the primaries (in our context this means to select either the BCP or the QBCP). Once this is accomplished, the selected model has to be completed including the effect of SRP on the sail. We refer to the resulting model to be the **augmented** version of the former. This nomenclature has already used in the literature, see [21]. There are several works in which the role of Sun's gravity in the Earth-Moon system is analyzed [22, 23, 24, 25, 26, 27, 8, 28, 29, 30, 10, 31]. In [32] we analyze two different models, the BCP and the QBCP. According to our conclusions, the QBCP is the suitable model to study the motion around the collinear points, specially the translunar point. While the BCP is suitable to undertake explorations near the triangular points. We build our models for the motion of a solar sail according to the conclusions of [32]. We use the Augmented Quasi-Bicircular Problem (AQBCP) to study the dynamics near the Lagrangian points L_1 and L_2 . The Augmented Bicircular Problem (ABCP) is used to study the motion of the triangular points and L_3 . The reason we study the collinear point L_3 together with the triangular ones will be made clear during the exposition of the results. These three (geometrically defined) points are related in a very specific way when the sail is added.

In the literature concerning to solar sails, most of the works do not take under consideration Sun's gravity.

The derivation of the mathematical formulation for SRP acting upon the sail can be found in several works, see for instance, [33, 34, 16, 20]. The direction of the acceleration due to SRP, denoted by the vector $s\vec{s}$, is given by:

$$\begin{aligned} s s^x &= \cos^3 \delta \cos^2 \alpha (\tilde{\alpha}_7 \cos \alpha + \tilde{\alpha}_8 \sin \alpha), \\ s s^y &= \cos^3 \delta \cos^2 \alpha (\tilde{\alpha}_7 \sin \alpha + \tilde{\alpha}_8 \cos \alpha), \\ s s^z &= \cos^2 \delta \cos^2 2\alpha \sin \delta. \end{aligned}$$

Here, $\tilde{\alpha}_i = \alpha_i / (\alpha_7^2 + \alpha_8^2)^{1/2}$, ω_S is Sun's frequency and $\delta, \alpha \in (-\pi/2, \pi/2)$ are angles relative to the Sun line. Both angles have physical sense when $\delta, \alpha \in [-\pi/2, \pi/2]$. If one of the two angles is set to $\pi/2$ or $-\pi/2$, SRP vanishes. Once we have an expression for SRP acceleration, we can add it to the equations of the restricted model, to complete it. The system is given by the periodic time dependent Hamiltonian function (with the same period as Sun, $T_S = 2\pi/\omega_S$):

$$\begin{aligned} H &= \frac{1}{2} \alpha_1 (p_x^2 + p_y^2 + p_z^2) + \alpha_2 (p_x x + p_y y + p_z z) \\ &+ \alpha_3 (p_x y - p_y x) + \alpha_4 x + \alpha_5 y \\ &- \alpha_6 \left(\frac{1-\mu}{r_{pe}} + \frac{\mu}{r_{pm}} + \frac{m_S}{r_{ps}} \right) - \frac{\beta m_S}{a_S^2} \langle s\vec{s}, \vec{e} \rangle. \end{aligned} \quad (1)$$

Here, the vector \vec{e} is given by $\vec{e} = (x, y, z)^T$. It is easy to see that the Hamiltonian function (1) has the symmetries

$$\begin{aligned} &(\theta, x, y, z, \dot{x}, \dot{y}, \dot{z}, \beta, \alpha, \delta) \\ &\mapsto (-\theta, x, y, -z, \dot{x}, \dot{y}, -\dot{z}, \beta, \alpha, -\delta), \end{aligned} \quad (2)$$

and

$$\begin{aligned} &(\theta, x, y, z, \dot{x}, \dot{y}, \dot{z}, \beta, \alpha, \delta) \\ &\mapsto (-\theta, x, -y, z, \dot{x}, -\dot{y}, \dot{z}, \beta, -\alpha, \delta), \end{aligned} \quad (3)$$

where $\dot{x} = p_x + y, \dot{y} = p_y - x, \dot{z} = p_z$.

Remark 2.1. The last discussion involves the periodic functions α_i 's presented in [7, 10] (see also [9, 35]). These functions are used to define the Hamiltonian of the QBCP. However, if we set,

$$\begin{aligned} \alpha_1 &= \alpha_3 = \alpha_6 = 1, & \alpha_2 &= 0, \\ \alpha_4 &= \frac{m_S}{a_S^2} \cos \theta, & \alpha_5 &= -\frac{m_S}{a_S^2} \sin \theta, \\ \alpha_7 &= a_S \cos \theta, & \alpha_8 &= -a_S \sin \theta, \end{aligned}$$

these values define the Hamiltonian of the BCP and, setting also $m_S = 0$, we obtain the RTBP. Therefore, the following formulation of the acceleration due to the SRP can be applied to the three models but using the corresponding values of the functions α_i 's. Notice that the mass of Sun m_S should not be taken zero when it multiplies the solar sail acceleration in the case of the ARTBP. We also point out that one of the angles defining the orientation of the sail is named α . This is rather an unfortunate notation that could be problematic only in the present section. We prefer to keep this notation, as it is used in previous works, and hope this will not confuse the reader.

2.1. Values of the parameters used in this work

Parameter β . The lightness number is the ratio between SRP and Sun's gravitational acceleration. It is used to quantify the effectivity of the sail. Real solar sails in space have achieved the following values: $\beta = 0.001$ (IKAROS), $\beta = 0.008$ (Nanosail) and $\beta = 0.011$ (LightSail-1). When $\beta = 1$ the magnitude of SRP acceleration (if the sail is perpendicular to the Sun) is the same as Sun's gravitational acceleration but in the opposite direction. If we name,

$$\beta = \frac{\sigma^*}{\sigma}, \quad \sigma^* = \frac{L_S}{2\pi G m_S c} \approx 1.53 \text{g/m}^2.$$

The quotient $\sigma = m/A$ is the sail loading parameter and parametrizes the performance of the Sail. We call char-

β	σ (g/m ²)	a_0 (mm/s ²)	Area (m ²)
0.01	153.0	0.059935	$\approx 8 \times 8$
0.02	76.5	0.119869	$\approx 12 \times 12$
0.03	51.0	0.179804	$\approx 14 \times 14$
0.04	38.25	0.239739	$\approx 16 \times 16$
0.05	30.6	0.359608	$\approx 20 \times 20$

Table 1: Relation between: β the sail lightness number, σ the inverse of the area-to-mass ratio of the satellite, a_0 the characteristic acceleration and A the sail area requirements for 10 kg of total mass [36].

acteristic acceleration to the acceleration experienced by the sail-craft at 1 AU. That is, if we have a space-craft mass of 10 kg we need a solar sail area of almost $14 \times 14 \text{ m}^2$ for a sail lightness number $\beta = 0.03$. In Table 1 we can see, for different sail lightness numbers β , the corresponding to inverse of the area-to-mass ratio (σ), the characteristic acceleration (a_0) and the required size of the solar sail for 10 kg of total space-craft mass. This means that a sail lightness number $\beta = 0.03$ corresponds to a characteristic acceleration of

0.179804 mm/s². Taking into account the current technology capabilities, we shall focus on moderate values $\beta \in [0, 0.1]$. These are values for which SRP has a remarkable impact on the natural dynamics of a spacecraft in the Earth-Moon system.

If we compare SRP acceleration with the Sun's gravity acceleration (in the BCP, for simplicity), we notice that the first is only a fraction (given by β) of the second. Therefore, a priori, it could seem that the contribution by Sun's gravity is much more important to the dynamics than the contribution by SRP. Nevertheless, this is not the case. Let us consider the series expansion of the Hamiltonian function of the BCP. The linear term is the same as the Coriolis term due to the motion of Earth-Moon barycentre but with opposite sign, see [32]. Therefore, the linear term and the Coriolis force cancel out and the contribution due to Sun's gravity starts at order two:

$$\frac{1}{a_S} \left(\frac{\rho}{a_S} \right)^2 P_2 \left(\frac{\cos(\theta)x - \sin(\theta)y}{\rho} \right) \sim \mathcal{O} \left(\frac{m_S}{a_S^3} \right) \approx 0.0056,$$

while the acceleration due to SRP is of order $\mathcal{O}(\beta \frac{m_S}{a_S^3}) \approx 2.17\beta$. Here, P_2 is the second Legendre polynomial and $\rho = x^2 + y^2 + z^2$. Therefore, SRP dominates Sun's gravity in the Earth-Moon System.

Parameters α and δ : These parameters define the orientation of the sail in space. The angle α directs acceleration within the plane of motion of the primaries. The angle δ directs out-of-plane acceleration if $\delta \neq 0$. In the case when $\delta = 0$ there is no out-of-plane acceleration. Therefore, the orbits that are confined in the plane of the primaries stay confined when the sail is added. To study these confined motion one can dispense with the vertical direction and the system can be considered a two degrees and a half Hamiltonian system. Indeed, the discussion presented in Section 5 is done in terms of a four dimensional stroboscopic map.

It is easy to see that, for a fixed value of β , the magnitude of SRP acceleration is maximized at $\alpha = \delta = 0$, while the maximum out-of-plane acceleration is given by $\pm \delta_{max} = \pm \sin^{-1}(1/\sqrt{3})$. Recall that if one of the two angles, α or δ , is set to $\pi/2$ or $-\pi/2$, SRP vanishes.

3. Mathematical preliminaries

In this section we review several mathematical notions and facts that will be used later in this paper. This is intended to make the reading easier. Let us consider a differential equation that depends periodically (with period T) in time. Let us name f the mapping

obtained from the evaluation of the flow at the period. This map is sometimes called mapping at period or **stroboscopic map**. These maps are the simplest kind of Poincaré maps, as the section is temporal, fixed and can be used to reduce the dimension of the whole phase-space by one. In periodic systems, there are no equilibrium points, the simplest invariant objects are the periodic orbits with the same period as the vector-field. Moreover, if γ is a periodic orbit with period T' , then $T' = mT$ for $m \in \mathbb{N} \setminus \{0\}$. Let us name minimal periodic orbits to those with period T . Minimal periodic orbits are fixed points of the stroboscopic map P , orbits whose period is a m -multiple of T are periodic points of period m .

The notion of stroboscopic map can be extended for vectorfields that depend on time in a quasi-periodic way. In this case, the dynamics of the map has two components: A part of the dynamics is an irrational rigid rotation taking place on a torus (the basis), the other part takes place on the phase space (the bundle).

If the vector-field is induced by a Hamiltonian function of m and a half degrees of freedom ($2m = n$), then the stroboscopic map is a **symplectic map**, i.e. for each z , the linearization of the map around z , $Df(z)$, verifies the following $Df(z)^t J Df(z) = J$, where

$$J = \begin{bmatrix} -I_m & 0 \\ 0 & I_m \end{bmatrix}$$

and I_m is the identity matrix of \mathbb{R}^m . This condition implies a number of interesting properties: Symplectic mappings are volume preserving, i.e. $\det(Df(z)) = 1$. The converse is only true if $m = 1$. The spectrum of a symplectic matrix is also tied by certain constrictions. In first place, if λ belongs to the spectrum of a symplectic matrix, then λ^{-1} also does. Moreover, each generic pair (λ, λ^{-1}) can be classified in the following stability types:

1. If λ has modulus different than one and it is real, the pair is said to be of hyperbolic (saddle) type.
2. If $\lambda = e^{i\theta}$, the pair is said to be of elliptic (centre) type.
3. If λ is complex and its modulus is different from one, it is part of a **Krein quartet** $(\lambda, \lambda^{-1}, \bar{\lambda}, \bar{\lambda}^{-1})$. The quartet is said to be of complex saddle type.

If the matrix $Df(z_0)^{j_0} - I_n$ is not invertible, for some $j_0 \in \mathbb{N}$, we say that z_0 is a bifurcating point. These points are not generic but appear when the system depends on parameters. The bifurcating points represent transitions between different stability types. Let us think that the eigenvalues are moving with respect some parameter. In

absence of degeneracies in higher order terms we have the following description:

1. **Saddle-Centre bifurcation:** A pair of elliptic eigenvalues meet at $\lambda = \lambda^{-1} = 1$, then, they abandon the unit circle along the real line. One of the eigenvalues starts being less than one and the other larger, both positive. In this case, the pair goes from elliptic type to hyperbolic. The reverse situation can happen as well, that is, two eigenvalues abandoning the real line and entering the unit circle through 1.
2. **Period Doubling bifurcation:** A pair of elliptic eigenvalues meet at $\lambda = \lambda^{-1} = -1$, then, they abandon the unit circle along the real line. One of the eigenvalues starts being less than -1 and the other larger, both negative. In this case, the pair goes from elliptic type to hyperbolic and two families of two-periodic elliptic points emerge from the collision. The opposite situation in which two families of doubled period merge with a family of fixed points and the last gains elliptic character is named period halving bifurcation.
3. **Krein Collision:** Two pair of elliptic eigenvalues meet at $\lambda = \lambda^{-1} = \bar{\lambda} = \bar{\lambda}^{-1} = e^{i\alpha}$, then all the eigenvalues get expelled from the unit circle. This has more complicated consequences. In the first place, the fixed point, after the bifurcation has 2D complex unstable and stable manifold. Then, depending on arithmetical properties of ρ it grows a family of q -period points (if $\alpha = \frac{2\pi}{q} \in \mathbb{Q}$) or a family of invariant curves. There are several aspects of this bifurcation that depend on higher order terms.

Some aspects of the dynamics around the fixed points can be inferred from its linear character. Under generic conditions, from the fixed point and along each plane associated to an elliptic pair, it grows a Cantorian family of invariant curves whose frequency tends to the (linear) frequency ρ of the pair [37]. This result can be regarded as the discrete version of the Lyapunov Centre Theorem for elliptic equilibria for autonomous Hamiltonian systems. In fact, more can be said: The nonlinear coupling of two different elliptic direction results in a Cantorian family of $2D$ invariant tori. If the point is totally elliptic, the nonlinear coupling of all the elliptic directions produces a set of maximal dimension of KAM tori that is what is expected around a totally elliptic fixed point [38].

4. Motion near L_1 and L_2

The dynamical structure around the Lagrangian points in the RTBP is well known [39, 40, 41]. For values of the mass parameter smaller than the Routh critical value, the collinear points (L_1 , L_2 and L_3) are of type saddle×centre×centre and the equilateral points L_4 and L_5 are of type centre×centre×centre.

The Lyapunov theorem (see [42]) states that, a family of periodic orbits grows along each elliptic eigen-space. These families can be parameterized by the frequency of the orbits, that tends to the normal mode of the equilibrium point as the family gets close to it. The orbits within these families are known as Lyapunov orbits. For each collinear point, there are two families of Lyapunov orbits (the horizontal and the vertical family). The horizontal families related to L_1 and L_3 can be continued up to trajectories which collide with Earth. The horizontal family corresponding to L_2 can be followed up to collisions with Moon. The vertical families finish in bifurcating planar orbits [43, 6]. The vertical and horizontal families met at a pitchfork bifurcation that leads to a new family of orbits, the Halo family [44, 45, 46, 6, 47].

On the other hand, the well known stable and unstable manifold Theorem states that, along each hyperbolic direction, there exist stable (unstable) manifolds, trajectories of the system that tend to the equilibrium point when time tends to infinity (minus infinity).

The models we deal in this paper are periodic perturbations of the RTBP. This means that the Lagrangian points are no longer equilibria but they are replaced by periodic orbits with the same period as the perturbation ($T_S = 2\pi/\omega_S$). In a similar way, the quasi-periodic structures (including the periodic orbits) gain, generically, the frequency ω_S . Consequently, most of the Lyapunov and Halo orbits are replaced by two dimensional invariant tori. The orbits that remain periodic under the perturbation of Sun are the resonant ones i.e. orbits whose period is a rational multiple of T_S .

In this section we focus on some Halo orbits related to the collinear points L_1 and L_2 . See [7, 8, 32] for a deep analysis of the orbits in the context of the QBCP. See also [20] for a further exploration of the orbits presented in this paper and other resonant orbits related to L_1 and L_2 . The orbits appearing in this paper are selected because their stabilization due to SRP is remarkable. We use the AQBCP to do so, indeed, as we explained before, it is a suitable model to study the motion near L_1 and L_2 . Let us give some words first concerning the QBCP: The periodic orbits that replace the collinear points L_1 and L_2 are highly unstable. Indeed, the largest eigenvalue of their corresponding monodromy matrices

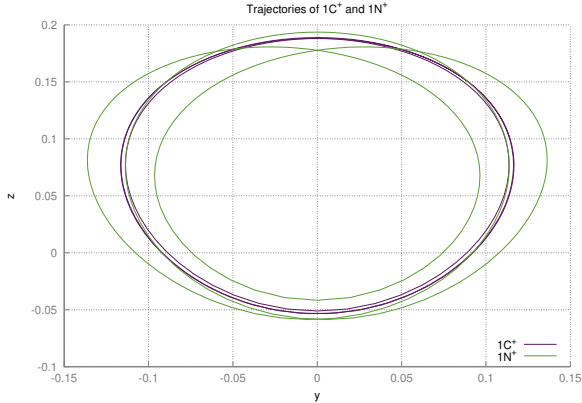


Figure 1: Trajectories of the Halo orbits $1C^+$ and $1N^+$ in the QBCP.

are of order 10^9 and 10^6 respectively. Most of the resonant periodic orbits near these equilibria are also highly unstable, see [7, 8].

Notice that, as the dynamical equivalents of L_1 and L_2 are small orbits which are close to their corresponding equilibrium point, we can estimate the size of the largest eigenvalue of the monodromy matrix of each orbit from the eigenvalues related to the equilibria. Indeed, if λ is the largest eigenvalue related to some equilibrium point (L_1 or L_2), then the largest eigenvalue of the monodromy matrix of the corresponding dynamical equivalent behaves as $\exp(\lambda T_S)$. Recall that T_S is the period of Sun and consequently the period of the dynamical equivalents.

4.1. Solar sail resonant Halo orbits near L_1

From the Halo family related to L_1 , we select two (1:3) resonant orbits: $1C^+$ (of linear character saddle \times centre \times centre) and $1N^+$ (of linear character saddle \times saddle \times centre), see Figure 1. The plus super-index indicates that those belong to the northern family. Of course, their symmetrical counterparts are denoted by $1C^-$ and $1N^-$.

To study how these orbits change with respect to the parameters of the sail we perform the following computation: fix $\alpha = 0$ and some value of β , then, continue the Halo orbits but regarded as fixed points of the stroboscopic map. In Figure 2 we observe the result of this continuation for $\beta = 0.01$, notice that, for visualization purposes, we display the trajectories of the flow (but the computation is done on the stroboscopic map). The green curve corresponds to $1C^+$ and the purple curve corresponds to $1N^+$. The blue dots correspond to intermediate curves. The continuation, therefore, establishes an homotopy between $1C^+$ and $1N^+$.

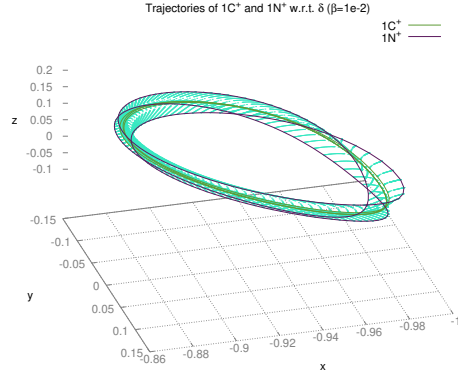


Figure 2: Continuation with respect to δ of $1C^+$ and $1N^+$. The parameter β is fixed at 0.01.

That is each value of $\delta \in [-\pi/2, \delta_{tp}^1]$ corresponds to a trajectory in Figure 2. Here the continuation is started at $\delta = -\pi/2$ and $1C^+$ and ends also for $\delta = \pi/2$ at $1N^+$. There is a turning point $\delta_{tp}^1 \approx -0.98$ where the linear character changes from saddle \times centre \times centre to saddle \times saddle \times centre. There are more bifurcations taking place in this continuation. In particular, there are orbits which are totally elliptic and of type complex saddle. That is, some of the blue curves pictured in dashed lines are stable. We want to point out that the range of values of δ for which the linear stability occurs is very narrow and not much relevant for practical purposes. However, the key phenomenon is that the largest eigenvalue decreases its size arbitrarily (until the orbits reach total ellipticity).

In Figure 3 we measure how the maximal eigenvalue of the orbits $1N^+$ and $1C^+$ (connected by continuation) change with respect to δ . We have five curves represented in Figure 3, those correspond to continuations (with respect to δ) for fixed values of $\beta = 0.01, 0.02, 0.03, 0.04$ and 0.05 . The curve on the left, the one that reaches the turning point for a largest value of $|\delta| \approx 1.33$, corresponds to $\beta = 0.05$. The rest of the curves are ordered according to the value of β (in decreasing order). The curve that has the turning point at δ_{tp}^1 corresponds to $\beta = 0.01$ i.e. those are the maximal eigenvalues in the trajectories displayed in Figure 2. In Figure 3, the horizontal axis shows the value of δ and the vertical axis the \log_{10} of the largest eigenvalue of the Monodromy matrix corresponding to each orbit. We notice that $1N^+$ (for $\delta = -\pi/2$, which corresponds to the QBCP) has a maximal eigenvalue of order 200. This means that an error in the orbit determination of 10^{-6} RTBP units

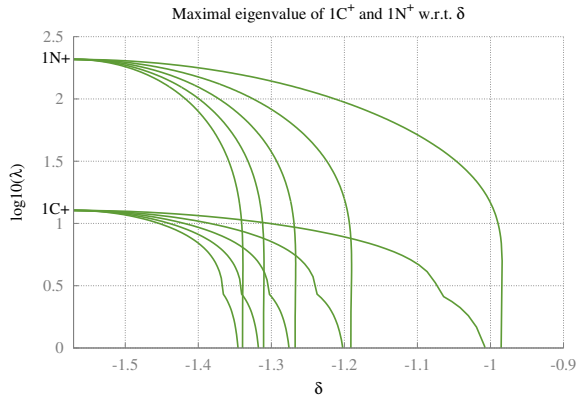


Figure 3: Maximal eigenvalue of the dynamical equivalents of $1C^+$ and $1N^+$ with respect to δ .

(about 1km) only needs approximately 10^{-2} RTBP time units (about 20 minutes) to get amplified to 1 RTBP unit (about 380000km). With the correct orientation of the sail, this propagation of error can be diminished as much as desired. A similar description holds for $1C^+$, which has smaller instability but of the same order.

4.2. Solar sail Halo resonant orbits near L_2

From the Halo family related to L_2 , we select a (1:2) resonant orbit: $2A^+$ (of linear character saddle \times saddle \times centre), see Figure 4. Again the super-index places the Halo orbit in the northern family and the symmetrical counterpart will be denoted by $2A^-$.

We perform the same simulation to understand how the Halo orbit $2A^+$ changes with respect to the parameters of the sail, that is, we fix a value of β and continue

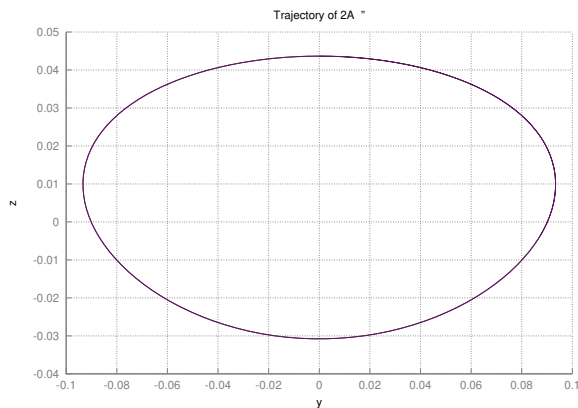


Figure 4: Trajectories of the Halo orbit $2A^+$ in the QBCP.

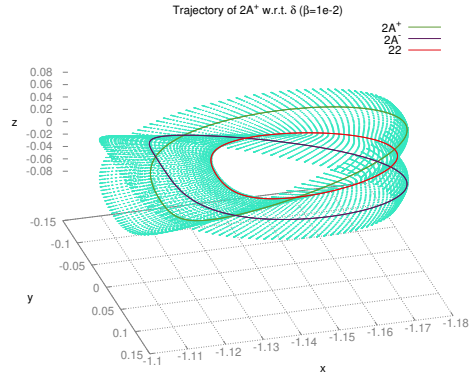


Figure 5: Continuation with respect to δ of $2A^+$ and $2A^-$. The parameter β is fixed at 0.01.

with respect to δ starting from $\delta = -\pi/2$ and stopping at $\delta = \pi/2$.

There are two typical behaviours for this continuation. If β is small enough, the continuation connects $2A^+$ with itself. There is a critical value of β^* for which, if $\beta > \beta^*$ the behaviour of the continuation is completely different: If we start a continuation at $2A^+$ for $\delta = -\pi/2$ and continue forward, the orbit increases its size and height (with respect to the plane of motion of the primaries) until $\delta = -\delta_{max}$, the orientation with maximal out-of-plane acceleration. After this point, the continuation turns down, to the plane, crossing it at a dynamical equivalent of a (1:2) resonant planar Lyapunov orbit. After crossing the plane, the continuation connects with the symmetrical counterpart $2A^-$ at $\delta = \delta/2$. If the continuation is performed backwards (starting at $\delta = \pi/2$ and decreasing the value of δ), the orbit $2A^-$ connects with the (1:2) resonant planar Lyapunov orbit of the QBCP for $\delta = -\pi/2$.

In Figure 5 we display the trajectories corresponding to the continuation with respect to δ for $\beta = 0.01$. The orbit $2A^+$ is depicted in green while its symmetric counterpart, $2A^-$ is colored in purple. The blue points represent the intermediate trajectories in the continuation (i.e. orbits corresponding to orientations $\delta \in (-\pi/2, \pi/2)$). The planar orbit in red corresponds to the Lyapunov resonant orbit. This trajectory is of linear type saddle \times centre \times centre. That is, there is a saddle-centre bifurcation before the continuation reaches the plane of motion of the primaries. Notice that, for $\delta = \pm\delta_{max}$ the dynamical equivalents are larger versions of $2A^+$ and $2A^-$ but much less unstable as we will explain.

In Figure 6 we show the change with respect to δ of

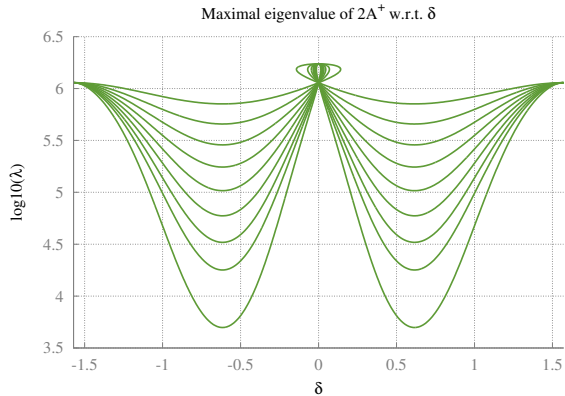


Figure 6: Maximal eigenvalue of the dynamical equivalents of $2A^+$ with respect to δ .

the maximal eigenvalue of the monodromy matrix of the orbits corresponding to $\beta = 0.01, 0.02, \dots, 0.1$. Notice that here we admit larger values of β in order to illustrate a remarkable decrease of the instability. Again, the horizontal axis stands for the orientation δ and the vertical axis is the \log_{10} of the largest eigenvalue. We observe that at $2A^+$, $2A^-$ and 22 , the dominant eigenvalue is close to a million. This means that an error in the orbit determination of 10^{-6} RTBP units (about 1km) only needs approximately 10^{-6} RTBP time units (about a tenth of second) to get amplified to 1 RTBP unit (about 380000km)

Unlike the dynamical equivalents of the Halo orbits near L_1 , here the trajectories are never stabilized. However it is remarkable that, selecting an orientation of the sail corresponding to the maximal out-of-plane acceleration (i.e. $\delta = \pm\delta_{max}$) one can decrease the size of the maximal eigenvalue remarkably. In particular, it can be reduced to the order of thousands for $\beta = 0.1$. Notice that, this means that an error of 1km in the determination of the orbit would correspond to an error of hundreds of km after a synodic month.

5. Motion near L_3 , L_4 and L_5

In this section we focus on the stable motion near the dynamical equivalents of the triangular points and L_3 when SRP is considered. Near these locations, the impact of SRP is enormously relevant as the lightness number increases, the position of the dynamical equivalents changes a lot. In this section the sail is taken to be perpendicular to Sun ($\delta = 0$ and $\alpha = 0$). All the studied orbits lie in the plane of motion of the primaries and

we dispense with the vertical direction and discuss the problem in the plane. The model we use is the ABCP.

It is well known that, in the BCP, the perturbation due to Sun gravity is large enough to produce bifurcations. In particular the triangular points are replaced by three periodic orbits (PO_1 , PO_2 and PO_3) caused by a broken pitchfork bifurcation. The orbit which is close to L_4 is small and slightly unstable. The remaining two are totally elliptic. The stable and unstable manifold of the hyperbolic orbit wander around the families of invariant tori growing from the elliptic directions of the stable orbits in a figure eight shape [32].

In Figure 7 we display the curve of fixed points corresponding to the continuation, with respect to β , of the dynamical equivalents of the triangular points (and L_3) in the BCP. The curve crosses $\beta = 0$ three times near L_4 (corresponding the three periodic orbits PO_1 , PO_2 , PO_3).

The numerical continuation uses PO_3 as initial condition. We observe that PO_3 can be continued for low positive values of β . Eventually the curve finds a turning point (changing from stable to unstable) and returns back to PO_1 . After another turning point, the curve regains stability and crosses again $\beta = 0$ at PO_2 . After that, the curve keeps tracking fixed points with positive values of β . Stress that fixed points with negative values of β do not have physical meaning but they are helpful to see that the three fixed points corresponding to the BCP are connected by the curve. All this process happens extremely fast in β .

Let β^1 ($\sim O(10^{-4})$) be the value of β for which the characteristic curve has the first turning point. For $\beta > \beta^1$, there is a single dynamical equivalent of L_4 , that is, there is exactly one fixed point continuing from PO_3 . The curve keeps going until it reaches the horizontal axis at β_2 (≈ 0.037). There, the characteristic curve undergoes a pitchfork bifurcation, and the branch corresponding to L_4 joins with the branches corresponding to L_3 and L_5 . For $\beta > \beta_2$ there exist a unique dynamical replacement for L_3 , L_4 and L_5 which is totally elliptic right after the bifurcation but changes its linear behaviour as β keeps increasing. At the same time, the trajectory (in the flow) corresponding to this unique dynamical replacement gets larger and, finally, it collides with Earth.

In Figure 7, the color of the curve represents the linear behaviour of the periodic orbit, the color code is given in the legend. We observe several changes of stability, they are product of the bifurcations. For $\beta \approx 2.75 \times 10^{-3}$, the characteristic curve undergoes a period doubling bifurcation. The main branch switches from stable to unstable and it creates two families of stable 2-periodic fixed points that eventually merge with the main branch

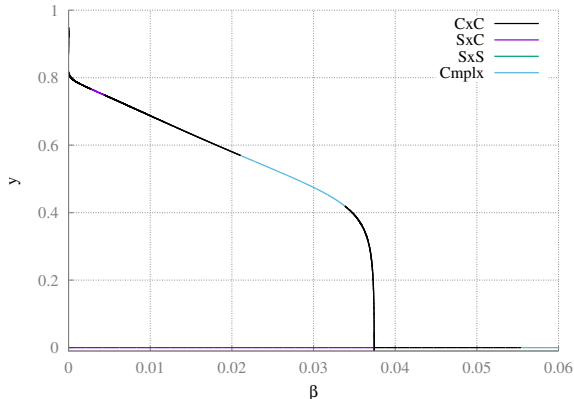


Figure 7: Dynamical equivalents of L_3 , L_4 and L_5 with respect to β and $\alpha = 0$.

in a period halving bifurcation. For $\beta \approx 2.1 \times 10^{-2}$, the characteristic curve undergoes a Hamiltonian-Hopf bifurcation and the main branch changes to complex instability. This is not a novelty as the same phenomenon is illustrated in [48, 16].

The consequence of the pitchfork bifurcation merging L_3 , L_4 and L_5 is that the dynamical equivalent of L_3 is stabilized. This means that a periodic orbit passing quite close to Earth is totally elliptic. As we have explained in Section 3, totally elliptic fixed points are surrounded by invariant tori. Moreover, close to the fixed point, these invariant tori are normally elliptic [49]. Normally elliptic invariant tori are sticky, i.e. trajectories close to them, need long times to move away. Therefore, it makes sense to look for regions of effective stability, regions in which the escape time is very large, around elliptic fixed points.

In Figure 8 we display a region $([0.085, 0.115] \times [-0.04, 0.04])$ of initial conditions around the only periodic orbit that replaces L_3 , L_4 and L_5 for $\beta = 0.04$. This orbit is totally elliptic and relatively close to Earth. The plot displayed in Figure 8 can be obtained as follows. First, produce a two dimensional grid in the plane (x, y) around the orbit (the velocities are fixed to the ones of the initial condition of the orbit). Second, take each initial condition of the grid and integrate it for $8000T_S$ units of time (this is the integration time used in other works [30, 48]). We control if the trajectory escapes (this means to abandon the region $[-0.1, 0.2] \times [-0.5, 0.5]$) and if the trajectory gets closer to Earth and Moon than their respective radii. Each initial condition is labeled according to its fate (1 if the trajectory collides with Earth, 2 if the trajectory collides with Moon, 3 if the trajectory escapes and 0 otherwise).

In Figure 8, the yellow points are initial conditions that escape, the purple ones collide with Earth and the red ones (located at the boundary between the purple and yellow points) collide with Moon. Finally the black points conform the region of effective stability, points that wander near Earth for a long time. The size of the stability region is about 5000km times 15000km. See also [48] for more details on the effect of SRP on stability regions near the triangular points and also for more details on how to compute these orbits.

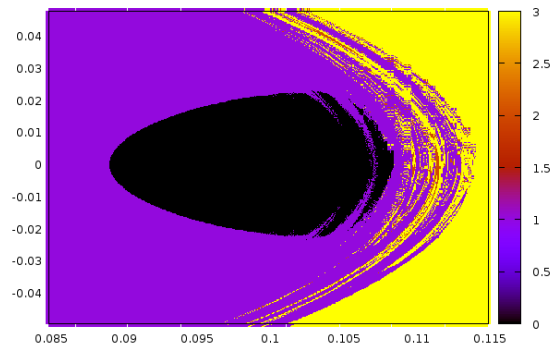


Figure 8: Initial conditions around the dynamical equivalent of L_3 , L_4 and L_5 corresponding to $\beta = 0.04$. Each initial condition has been integrated $8000T_S$ units of time. Yellow points: Escape. Purple points: Collide with Earth. Red points: Collide with Moon. Black points: Stability region. Horizontal axis: x . Vertical axis: y .

6. Conclusions

In this paper we have considered two models for the motion of a solar sail in the Earth-Moon system. Both consider the gravitational effects of Earth, Moon and Sun, as well as the effect of SRP on the sail. The ABCP is a suitable model to study the motion near the triangular points and L_3 , while the AQBCP is considered to study the motion near L_1 and L_2 . Although the AQBCP could be used as well to study the motion near the triangular points, as the results are qualitatively similar, we use the ABCP because some computations present in this paper require long integrations and the ABCP has, computationally speaking, a much cheaper vectorfield to evaluate, see [32].

Using the AQBCP, we have shown that a couple of resonant Halo orbits that are related to L_1 can be stabilized by means of a Sail. This is achieved with a not so large value of the effectivity ($\beta = 0.01$) and a sail pitched vertically. Also using the same model, we have shown that a resonant Halo orbit related to the translunar point can be made less unstable, decreasing the largest

eigenvalue of its monodromy matrix a couple of orders. To do this, the effectivity of the sail must be larger (about $\beta = 0.1$). We have also seen that the smallest value of the maximal eigenvalue takes place when the orientation of the sail maximizes the out-of-plane acceleration.

In the case of the triangular points and L_3 the effect of SRP in the sail is even more remarkable. SRP stabilizes the dynamical equivalent of L_4 for very small values of β . It also changes the size and the shape of the periodic orbit and produces several bifurcations. A remarkable one takes place for a sail perpendicular to Sun, where L_3 , L_4 and L_5 merge in a pitchfork bifurcation. As a result, L_3 is stabilized and a region of effective stability close to Earth appears for β about 0.037.

7. Technical details

The integrations of this work have been carried out using a Taylor method [50] with variable order and step-size. The required local accuracy for the integrations has been 10^{-16} . Due to the highly unstable character of some orbits, it has been mandatory to use a multiple shooting approach to compute most of the periodic orbits. A maximum of four sections has been required. All the periodic orbits have been computed with accuracy higher than 10^{-12} . The continuation method we use is the pseudo arclength method with a Newton scheme as a corrector. The differential of the stroboscopic (necessary to compute the orbits and study their stability) is obtained by using Jet Transport [51, 52]. All the programs used to perform the computations of this work have been written in C from the scratch. Files containing the values of the parameters used in this work can be found at <http://www.maia.ub.edu/~marc/EMQBCP>

Acknowledgments

This work has been supported by the Spanish grants PGC2018-100699-B-I00 (MCIU/AEI/FEDER, UE) and the Catalan grant 2017 SGR 1374. The project leading to this application has received funding from the European Union's Horizon 2020 research and innovation programme under the Marie Skłodowska-Curie grant agreement No 734557.

References

[1] R. Vondrak, J. Keller, G. Chin, and J. Garvin. Lunar reconnaissance orbiter LRO: Observations for Lunar exploration and science. *Space Science Reviews*, 150(1):7–22, Jan 2010. ISSN 1572-9672. doi: 10.1007/s11214-010-9631-5.

[2] T. Sweetser, S. Broschart, V. Angelopoulos, G. Whiffen, D. Folta, M. Chung, S. J. Hatch, and M. Woodard. ARTEMIS mission design. *Space Science Reviews*, 165:27–57, 09 2011. doi: 10.1007/s11214-012-9869-1.

[3] V. Sundararajan. Overview and technical architecture of India's Chandrayaan-2 mission to the Moon. In *Proceedings of the AIAA Aerospace Sciences Meeting*, Kissimmee, US, 8–12 January 2018.

[4] S.S. Huang. *Very restricted four-body problem*. NASA technical note. National Aeronautics and Space Administration, 1960. URL <https://books.google.es/books?id=ikiSsmF5smisC>.

[5] J. Cronin, P.B. Richards, and L.H. Russell. Some periodic solutions of a four-body problem. *Icarus*, 3:423–428, 1964.

[6] G. Gómez, À. Jorba, J. Masdemont, and C. Simó. Study refinement of semi-analytical Halo orbit theory. ESOC contract 8625/89/D/MD(SC), final report, European Space Agency, 1991. Reprinted as *Dynamics and mission design near libration points. Vol. III, Advanced methods for collinear points*, volume 4 of World Scientific Monograph Series in Mathematics, 2001.

[7] M.A. Andreu. *The quasi-bicircular problem*. PhD thesis, Univ. Barcelona, 1998.

[8] M.A. Andreu and C. Simó. The quasi-bicircular problem for the Earth-Moon-Sun parameters. Preprint, 2000.

[9] F. Gabern and À. Jorba. A restricted four-body model for the dynamics near the Lagrangian points of the Sun-Jupiter system. *Discrete Contin. Dyn. Syst. Ser. B*, 1(2):143–182, 2001.

[10] M.A. Andreu. Dynamics in the center manifold around L_2 in the quasi-bicircular problem. *Celestial Mech.*, 84(2):105–133, 2002.

[11] C. R. McInnes. Solar sail trajectories at the lunar L_2 Lagrange point. *Journal of Spacecraft and Rockets*, 30(6):782–784, 1993.

[12] M. T. Ozimek, D. J. Grebow, and K. C. Howell. Design of solar sail trajectories with applications to Lunar south pole coverage. *Journal of Guidance, Control, and Dynamics*, 32(6):1884–1897, 2009.

[13] X. Hou, J. Tang, and L. Liu. On utilization of solar sails in triangular libration point missions in the Earth-Moon system. *Transactions of the Japan society for aeronautical and space sciences, aerospace technology japan*, 8(ists27):1–5, 2009. doi: 10.2322/tastj.8.Td.1.

[14] G. Wawrzyniak and K. C. Howell. Generating solar sail trajectories in the Earth-Moon system using augmented finite-difference methods. *International Journal of Aerospace Engineering*, page 13 pages, 2011. Article ID 476197.

[15] J. Heiligers, M. Macdonald, and J. S. Parker. Extension of Earth-Moon libration point orbits with solar sail propulsion. *Astrophysics and Space Science*, 361(7):1–20, 2016.

[16] M. Jorba-Cuscó, A. Farrés, and À. Jorba. Periodic and quasi-periodic motion for a solar sail in the Earth-Moon system. In *Proceedings of the 67th International Astronautical Congress*, Guadalajara, México, 26–30 September 2016.

[17] R. Sood and K. C. Howell. L_4 , L_5 solar sail transfers and trajectory design: Solar observations and potential Earth Trojan exploration. In *Proceedings of the 26th AAS/AIAA Space Flight Mechanics Meeting*, 2016.

[18] C.R. McInnes, A.J.C. McDonald, J.F.L. Simmons, and E.W. MacDonal. Solar sail parking in restricted three-body system. *Journal of Guidance, Control and Dynamics*, 17(2):399–406, 1994.

[19] A. Farrés and À. Jorba. A dynamical system approach for the station keeping of a solar sail. *J. Astronaut. Sci.*, 56(2):199 – 230, 2008.

[20] M. Jorba-Cuscó, A. Farrés, and À. Jorba. Solar sail resonant periodic orbits in the augmented Earth-Moon Quasi-Bicircular

- Problem. In *Proceedings of the 69th International Astronautical Congress*, Bremen, Germany, 1–5 October 2018.
- [21] A. Farrés, À. Jorba, and J. M. Mondelo. Numerical study of the geometry of the phase space of the augmented hill three-body problem. *Celestial Mechanics and Dynamical Astronomy*, 129(1):25–55, Sep 2017. ISSN 1572-9478. doi: 10.1007/s10569-017-9762-z. URL <https://doi.org/10.1007/s10569-017-9762-z>.
- [22] B.E. Schutz and B.D. Tapley. Numerical studies of solar influenced particle motion near the triangular Earth-Moon libration points. In G.E.O Giacaglia, editor, *Periodic Orbits, Stability and Resonances*, pages 128–142. D. Reidel Publishing Company, Dordrecht, Holland, 1970.
- [23] G. Gómez, J. Llibre, R. Martínez, and C. Simó. Station keeping of libration point orbits. ESOC contract 5648/83/D/JS(SC), final report, European Space Agency, 1985. Reprinted as *Dynamics and mission design near libration points. Vol. I, Fundamentals: the case of collinear libration points*, volume 2 of World Scientific Monograph Series in Mathematics, 2001.
- [24] G. Gómez, À. Jorba, J. Masdemont, and C. Simó. A quasiperiodic solution as a substitute of I_4 in the Earth-Moon system. In *Proceedings of the 3rd International Symposium on Spacecraft Flight Dynamics*, pages 35–41, ESTEC, Noordwijk, Holand, 1991. ESA Publications Division. ISBN 92-9092-146-3.
- [25] G. Gómez, À. Jorba, J. Masdemont, and C. Simó. Quasiperiodic orbits as a substitute of libration points in the solar system. In A.E. Roy, editor, *Predictability, Stability and Chaos in N-Body Dynamical Systems*, pages 433–438. Plenum Press, 1991.
- [26] G. Gómez, À. Jorba, J. Masdemont, and C. Simó. Study of Poincaré maps for orbits near Lagrangian points. ESOC contract 9711/91/D/IM(SC), final report, European Space Agency, 1993. Reprinted as *Dynamics and mission design near libration points. Vol. IV, Advanced methods for triangular points*, volume 5 of World Scientific Monograph Series in Mathematics, 2001.
- [27] C. Simó, G. Gómez, À. Jorba, and J. Masdemont. The Bicircular model near the triangular libration points of the RTBP. In A.E. Roy and B.A. Steves, editors, *From Newton to Chaos*, pages 343–370, New York, 1995. Plenum Press.
- [28] G. Gómez, J. Llibre, R. Martínez, and C. Simó. *Dynamics and mission design near libration points. Vol. I, Fundamentals: the case of collinear libration points*, volume 2 of *World Scientific Monograph Series in Mathematics*. World Scientific Publishing Co. Inc., 2001. ISBN 981-02-4285-9.
- [29] E. Castellà and À. Jorba. On the vertical families of two-dimensional tori near the triangular points of the Bicircular problem. *Celestial Mech.*, 76(1):35–54, 2000.
- [30] À. Jorba. A numerical study on the existence of stable motions near the triangular points of the real Earth-Moon system. *Astron. Astrophys.*, 364(1):327–338, 2000.
- [31] B. L. Bihan, J. Masdemont, G. Gómez, and S. Lizy-Destrez. Invariant manifolds of a non-autonomous quasi-bicircular problem computed via the parameterization method. *Nonlinearity*, 30(8):3040, 2017. URL <http://stacks.iop.org/0951-7715/30/i=8/a=3040>.
- [32] M. Jorba-Cuscó, A. Farrés, and À. Jorba. Two periodic models for the Earth-Moon system. *Frontiers in Applied Mathematics and Statistics*, 4:32, 2018. ISSN 2297-4687. doi: 10.3389/fams.2018.00032. URL <https://www.frontiersin.org/article/10.3389/fams.2018.00032>.
- [33] C.R. McInnes. *Solar Sailing: Technology, Dynamics and Mission Applications*. Springer-Praxis, 1999.
- [34] A. Farrés, À. Jorba, and M. Jorba-Cuscó. On the solar sail periodic orbits near the Earth-Moon libration points. In *Proceedings of the XXIV Congress on differential equations and applications*, Cádiz, Spain, 8–12 June 2015.
- [35] F. Gabern. *On the dynamics of the Trojan asteroids*. PhD thesis, Univ. de Barcelona, 2003.
- [36] B. Dachwald, W. Seboldt, M. Macdonald, G. Mengali, A.A. Quarta, C.R. McInnes, L. Rios-Reyes, D.J. Scheeres, B. Wie, M. Görlich, et al. Potential Solar Sail Degradation Effects on Trajectory and Attitude Control. In *AIAA Guidance, Navigation, and Control Conference and Exhibit*, volume 6172, 2005.
- [37] À. Jorba and J. Villanueva. On the persistence of lower dimensional invariant tori under quasi-periodic perturbations. *J. Nonlinear Sci.*, 7:427–473, 1997.
- [38] R. de la Llave, A. González, À. Jorba, and J. Villanueva. KAM theory without action-angle variables. *Nonlinearity*, 18(2):855–895, 2005.
- [39] H. Poincaré. Sur le problème des trois corps et les équations de la dynamique. *Acta Math.*, 13:1–271, 1890.
- [40] H. Poincaré. *Les méthodes nouvelles de la mécanique céleste*, volume 1, 2, 3. Gauthier-Villars, Paris, 1892–1899.
- [41] V. Szebehely. *Theory of Orbits*. Academic Press, 1967.
- [42] K.R. Meyer and G.R. Hall. *Introduction to Hamiltonian Dynamical Systems and the N-Body Problem*. Springer, New York, 1992.
- [43] J.M. Mondelo. *Contribution to the study of Fourier methods for quasi-periodic functions and the vicinity of the collinear libration points*. PhD thesis, Univ. Barcelona, 2001.
- [44] R.A. Broucke. *Periodic Orbits in the Restricted Three-body Problem with Earth-Moon Masses*. JPL technical report. Jet Propulsion Laboratory, California Institute of Technology, 1968. URL <https://books.google.es/books?id=ZB8HGQAACAAJ>.
- [45] R. W. Farquhar and A. A. Kamel. Quasi-periodic orbits about the translunar libration point. *Celestial mechanics*, 7(4):458–473, Jun 1973. ISSN 1572-9478. doi: 10.1007/BF01227511. URL <https://doi.org/10.1007/BF01227511>.
- [46] J. V. Breakwell and J. V. Brown. The ‘Halo’ family of 3-dimensional periodic orbits in the Earth-Moon restricted 3-body problem. *Celestial mechanics*, 20(4):389–404, Nov 1979. ISSN 1572-9478. doi: 10.1007/BF01230405. URL <https://doi.org/10.1007/BF01230405>.
- [47] G. Gómez and J.M. Mondelo. The dynamics around the collinear equilibrium points of the RTBP. *Phys. D*, 157(4):283–321, 2001.
- [48] M. Jorba-Cuscó, A. Farrés, and À. Jorba. A study on the effect of solar radiation pressure on the stability region near the Earth-Moon triangular points. In *Proceedings of the 66th International Astronautical Congress*, Jerusalem, Israel, 12–16 October 2015.
- [49] À. Jorba and J. Villanueva. On the normal behaviour of partially elliptic lower dimensional tori of Hamiltonian systems. *Nonlinearity*, 10:783–822, 1997.
- [50] À. Jorba and M. Zou. A software package for the numerical integration of odes by means of high-order taylor methods. *Experimental Mathematics*, 14(1):99–117, 2005.
- [51] J. Gimeno, À. Jorba, M. Jorba-Cuscó, N. Miguel, and M. Zou. Numerical integration of high order variational equations of ODE’s. Preprint, 2018.
- [52] D. Pérez-Palau, J. Masdemont, and G. Gómez. Tools to detect structures in dynamical systems using jet transport. *Celestial Mechanics and Dynamical Astronomy*, 123(3):239–262, Nov 2015. ISSN 1572-9478. doi: 10.1007/s10569-015-9634-3. URL <https://doi.org/10.1007/s10569-015-9634-3>.